Journal Pre-proofs

Redox Flow Desalination based on the Temperature Difference as a Driving Force

Jinhong Dai, Mingzhi Huang, Kwan San Hui, Denis Y. W. Yu, Dongliang Yan, Kwun Nam Hui, Swee Ching Tan, Liguo Zhang, Fuming Chen

PII: S1385-8947(20)33837-7
DOI: https://doi.org/10.1016/j.cej.2020.127716
Reference: CEJ 127716

To appear in: *Chemical Engineering Journal*

Received Date: 18 August 2020
Revised Date: 31 October 2020
Accepted Date: 10 November 2020

Please cite this article as: J. Dai, M. Huang, K. San Hui, D. Y. W. Yu, D. Yan, K. Nam Hui, S. Ching Tan, L. Zhang, F. Chen, Redox Flow Desalination based on the Temperature Difference as a Driving Force, *Chemical Engineering Journal* (2020), doi: https://doi.org/10.1016/j.cej.2020.127716

Redox Flow Desalination based on the Temperature Difference as a Driving Force

Jinhong Dai[1,2], Mingzhi Huang[3], Kwan San Hui[4], Denis Y. W. Yu[5], Dongliang Yan[6], Kwun Nam Hui[7], Swee Ching Tan[8], Liguo Zhang[3], Fuming Chen[1,2]*

[1] *Guangdong Provincial Key Laboratory of Quantum Engineering and Quantum Materials, School of Physics and Telecommunication Engineering, South China Normal University, Guangzhou 510006, P.R. China*

[2] *Guangdong-Hong Kong Joint Laboratory of Quantum Matter, Frontier Research Institute for Physics, South China Normal University, Guangzhou 510006, China*

[3] *Guangdong Provincial Key Laboratory of Chemical Pollution and Environmental Safety & MOE Key Laboratory of Theoretical Chemistry of Environment, School of Environment, South China Normal University, Guangzhou 510006, PR China*

[4] *Engineering, Faculty of Science, University of East Anglia, Norwich, UK*

[5] *School of Energy and Environment, City University of Hong Kong, Tat Chee Avenue, Kowloon, Hong Kong Special Administrative Region*

[6] *School of Material Science and Engineering, Guilin University of Electronic Technology, Guilin, 541004, China*

[7] *Joint Key Laboratory of the Ministry of Education, Institute of Applied Physics and Materials Engineering, University of Macau, Avenida da Universidade, Taipa, Macau, PR China*

[8] *Department of Materials Science and Engineering, National University of Singapore, 9 Engineering Drive 1, Singapore 117574, Singapore*

* Email: fmchen@m.scnu.edu.cn (F. Chen)

ABSTRACT

How to effectively reduce the consumption of electrical energy is a key topic in many studies of electrochemical desalination. In this work, we use the temperature difference to drive a continuous process of dialysis desalination. The system consists of a thermoelectric unit and a desalination unit connected in series. The thermoelectric unit includes a thermoelectric generator (TEG), a heater as heat source and an air-cooled heat sink to generate electricity and for the desalination unit. The desalination unit

contains two platinum-coated hydrophobic carbon cloths as current collectors, a mixture of $[Fe(CN)_6]^{3-/4-}$ as anolyte and catholyte, concentrated and diluted salt streams with two cationic and one anionic exchange membranes separated configuration (CEM|AEM|CEM). During the charging process driven by temperature difference, chloride and sodium ions in the diluted salt stream move to the concentrated salt stream and cathodic reservoir, respectively. The results show that the concentration of brine drops significantly from 5,000 ppm to 344.3 ppm as the current decreases to 0.06 mA from the initial 1.30 mA when the temperature difference is maintained at 65 K. Concurrently, the average salt removal rate is up to 8.8 μg cm^{-2} min^{-1} and average heat consumption is 284.3 MJ $mole^{-1}$. Moreover, the influences from the temperature difference, salt feeds content and electrolyte concentration are also investigated in detail. This research has the potential application for the freshwater obtainment via the utilization of waste heat, and will be significant in places with the shortage of the electrical energy such as ships, islands and oceans with the temperature differences.

Keywords: Redox flow desalination; electrochemical desalination; water treatment; energy consumption; thermo drive

1. INTRODUCTION

The continuous growth of population and the rapid development of society have aggravated the pollution of global water resources,[1, 2] resulting in a shortage of fresh water resources in many regions.[3-5] To solve this problem, desalination is considered as one of the most effective ways to provide fresh water.[6] As a mature seawater desalination process, electrodialysis has been applied in large industrial production of portable water from brackish water sources for more than half a century with simple process and convenient operation.[7, 8] However, conventional electrodialysis desalination technology consumes much electrical energy. In order to reduce the energy consumption, many methods have been explored, such as the synthesis of less resistance and highly selective ion exchange membrane[9, 10] and the investigation of membrane-free[11] or low-voltage electrode material[12-15] and the choice of redox electrolyte[16, 17]. In particular, the electrodialysis desalination system using a redox mediator has received growing attention as an emerging desalination technology. For instance, Chen et al. proposed a continuous electrodialysis desalination technology based on metal-free organic redox electrolyte in 2019[18], and subsequently presented the use of riboflavin-5′-phosphate sodium salt[19] and methyl viologen[20] to achieve redox flow continuous desalination with less environmental pollution and low energy consumption, respectively. Choi et al. use the oxidation and reduction of the same redox couple with the fast redox kinetics as the anode and cathode reactions of an electrodialysis (ED) cell[21], which reduces the thermodynamic equilibrium cell potential and the kinetic overpotentials required for cell operation. Further, some studies have coupled electrodialysis desalination with reverse electrodialysis which collects the salinity gradient power to provide the driving force for electrodialysis desalination, thereby achieving energy self-sufficiency throughout the process.[22-24]

Similarly, if we convert other usable and readily available or waste energy sources into electrical energy and supply it to the redox flow desalination unit, this will reduce supplied energy during the process of electrodialysis desalination.

Thermo-driven electrochemistry is a scalable technology that makes use of the temperature difference between hot and cold sides of a thermoelectric generator (TEG) to generate electricity. It is widely applied to energy production, electrical catalysis and other fields due to the direct conversion of waste heat into useful electricity.[25-30] However, thermal power generation has not been applied in the redox flow desalination yet.

Herein, we propose a method for continuous dialysis desalination based on the temperature difference as driving force, which provides power for desalination reaction by thermoelectric conversion through thermoelectric materials. Our model system is composed of two parts in series: the thermoelectric unit functioning as a power supply and the desalination unit with ions movement. The main component of the thermoelectric unit is a TEG device that converts the thermal energy into the electrical energy. The heater and air-cooled heat sink are respectively placed on the hot and cold sides of TEG to simulate the formation of temperature difference. When the heater and air-cooled heat sink are working, the carriers near the hot side of TEG have higher kinetic energy than those near the cold side, and the number of carriers that are thermally excited to enter the conduction band or valence band near the hot side is also greater than that near the cold side, so that the carriers migrate from hot side to cold side inside the TEG. Thereby, a self-built electric field is formed inside the TEG to hinder this migration, and the Seebeck potential is generated. The electromotive force generated by TEG will provide electricity for desalination unit attributed to the series connection of TEG and desalination unit. Under the action of this driving force, the desalination unit involving a recirculated redox electrolyte of $[Fe(CN)_6]^{3-/4-}$, diluted and

concentrated salt streams with three membranes is equivalent to an electrolytic cell denoted as "(Anode)$[Fe(CN)_6]^{3-/4-}$ | CEM | Concentrated Stream | AEM | Diluted Stream | CEM | $[Fe(CN)_6]^{3-/4-}$(Cathode)". The $[Fe(CN)_6]^{4-}$ ions in the anodic reservoir are oxidized by releasing electrons which are captured by the $[Fe(CN)_6]^{3-}$ ions in the cathodic reservoir through the external circuit, resulting in the reduction of $[Fe(CN)_6]^{3-}$ ions at cathode. To compensate the electrostatic balance, the chloride and sodium ions in diluted salt stream move to the concentrated salt stream through the middle AEM and to the cathodic reservoir via CEM on the cathode side, respectively, which decreases the salt concentration of the diluted stream. The average desalination rate, heat consumption, thermoelectric conversion efficiency, electricity utilization efficiency, and thermoelectric utilization efficiency were investigated. In addition, the temperature difference determines the electromotive force of TEG, various initial salt concentration and electrolyte concentration will directly influence the resistance of the desalination unit. The current desalination system can also be combined with other waste heat emission processes such as exhaust heat of factories/engines, or utilize the temperature differences of interior and exterior ships, islands or oceans to solve the energy consumption problem in electrochemical desalination application.

2. MATERIALS AND METHODS

2.1 Materials, electrode fabrication, and solution preparation

The Bi_2Te_3 based thermoelectric generator (TEG, TEC1-0706) with a size of $40\ mm \times 40\ mm \times 3.9\ mm$ was ordered from Tianjin Haote Technology Co. Ltd, which is made of 7 pairs of series connected p-n thermocouple with a cross-sectional area of $1.4 \times 1.4\ mm^2$ and a height of $1.6\ mm$ ($A_{pn} = A_P = A_n = 1.4 \times 1.4\ mm^2$, $L_{pn} = L_p = L_n = 1.6\ mm$). Both materials of p-type and n-type are Bi_2Te_3. The heater

(LC-DMS-H), the copper heat sink, thermal grease (GD66), and air-cooled equipment (WY-F4) were the commonly used. Potassium ferricyanide (99 %), potassium ferrocyanide (99.5 %) and sodium chloride (99.5 %) were from Sigma-Aldrich and used without further purification. Pt/C catalyst (20/80, Vulcan XC-72) was from Beijing nano-catalyst Technology Co. Ltd. The ion exchange membranes (AEM/CEM, standard grade) were from Tokuyama, Japan. The current collectors were made of two hydrophobic carbon cloths (W1S1009, Tai Wan) coated with an N-methyl-2-pyrrolidone (NMP) slurry containing Pt/C and polyvinylidene fluoride (PVDF) at the mass ratio of 85 to 15 together with graphite papers. The carbon cloths were dried in a vacuum oven at 60℃ for one day before use. $[Fe(CN)_6]^{3-/4-}$ solution was prepared by adding 2 mmol $[Fe(CN)_6]^{3-}$, 2 mmol $[Fe(CN)_6]^{4-}$ and 0.5 g NaCl into 100 mL deionized water to prepare 20 mM/20 mM electrolyte. A total of 5 mL $[Fe(CN)_6]^{3-/4-}$ solution was used as the anolyte and catholyte. 0.5 g NaCl was dissolved into 100 mL deionized water to prepare 5000 ppm salt feed. Two 3 mL of NaCl solution were used as the test feeds. Before the desalination tests, all solvents were purged with pure N_2 to remove dissolved air.

2.2 Experimental setup

As displayed in **Figure S1** in the Supporting Information, the desalination system driven by temperature difference consists of a thermoelectric unit and a desalination unit connected in series. The thermoelectric unit includes a TEG, a heater as heat source, an air-cooled heat sink to produce temperature difference. The hot side of TEG is put on the center of the heater with thermal grease, while an air-cooled heat sink is placed on the cold side with thermal grease. The desalination unit is composed of two platinum-coated hydrophobic carbon cloths as current collectors, a mixture of $[Fe(CN)_6]^{3-/4-}$ as anolyte and catholyte, concentrated and diluted salt streams with three

membranes. The AEM is located between salt stream 1 and 2, while two CEMs are placed between the salt streams and anodic/cathodic reservoir, as the schematic diagram shown in **Figure 2a**. The 20 mM/20 mM $[Fe(CN)_6]^{3-/4-}$ electrolyte in 5 mL solution flows with 17.28 mL min^{-1} in the anodic and cathodic chambers connected to each other using a soft tube, then circles back to the container. The salt feeds of the two channels (5000 ppm each with 3 mL NaCl solution) are separately circulated. The $[Fe(CN)_6]^{3-/4-}$ electrolyte and two salt streams are driven using peristaltic pumps. Each compartment chamber of electrolyte or salt feeds has a cuboid dimension with $0.3\ cm$ height and $1.5 \times 1.5\ cm^2$ cross-sectional area i.e. the active area during desalination. Except for the two outermost sheets, which are acrylic plates, the other sheets are made of silica rubber material.

2.3 Desalination tests driven by temperature difference

Since the desalination process is driven by the temperature difference, various desalination effects can be achieved by adjusting the temperature difference between the hot and cold sides of TEG. The greater the temperature difference, the higher the Seebeck potential of TEG. For the same series circuit, the generated current which influences the rate of electron transfer in the desalination unit becomes larger, so that the desalination performance is affected. Due to the recirculation of $[Fe(CN)_6]^{3-/4-}$ redox electrolyte in the cathodic and anodic reservoirs, the sodium ions moving to the cathodic reservoir will flow to the anodic reservoir and be transferred to the concentrated salt stream through CEM of the anode side, lead to an increased salinity in the concentrated stream. The salt of the diluted stream is gradually transferred to the concentrated stream in whole desalination process driven by temperature difference. The conductivities of salt feeds in stream 1 and 2 were separately recorded in real time by two conductivity meters (eDAQ, EPU357). According to the salt concentration

corresponding to each conductivity, the conversion relationship between the conductivity and concentration of salt stream is obtained in the range of conductivity before and after desalination, following by substituting the conductivity into the conversion formula to obtain the corresponding salt concentration. The current and voltage of desalination unit were monitored by an electrochemical workstation (CHI760E, CH Instruments, Ins, USA) and a battery analyzer (Neware, BTS-4000) respectively. The three streams were recirculated separately with three single-channel peristaltic pumps (NKCP-S04B, B9M0815658). The compositional change of electrolyte containing $[Fe(CN)_6]^{3-}$/$[Fe(CN)_6]^{4-}$ during cell operation was determined by detecting the absorption spectra of electrolyte before and after desalination with an ultraviolet-visible spectrophotometer (SHIMADZU, UV-2600).

For continuous desalination test, the temperature difference between two sides of TEG was set to 65 K of which the hot and cold side temperatures were 363 K and 298 K, respectively. The initial salt concentration was 5000 ppm and the temperature are maintained until the salt concentration in stream 2 was minimized with the limited salt content. The electrolyte concentration was 20 mM. In the performance tests of temperature change, the temperature differences were controlled at 20 K, 35 K, 50 K and 65 K, respectively (hot side temperatures were separately 318 K, 333 K, 348 K, 363 K and cold side in each test was kept around 298 K). To further study the influence of concentration in salt feeds and $[Fe(CN)_6]^{3-/4-}$ electrolyte, the initial concentrations of feeds and electrolyte were adjusted to 1000 ppm, 3000 ppm, 5000 ppm, 7000 ppm, and 5 mM, 10 mM, 20 mM, 40 mM, respectively.

2.4 Performance parameters of thermo driving desalination

In order to understand the related parameters more clearly, **Figure 1** presents an energy flow sketch during the redox flow desalination based on the temperature difference as

driving force.

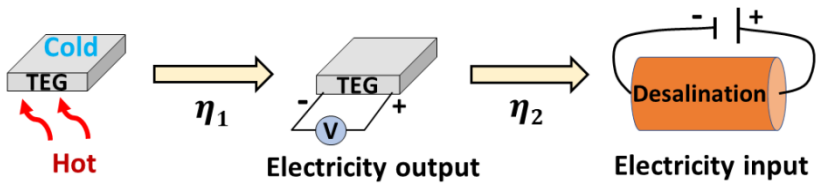

Figure 1. The energy flow sketch during the desalination driven by temperature difference.

Parameters			
c_0	initial concentration of salt stream (ppm)	K	thermal conductance (W K^{-1})
c_t	final concentration of salt stream (ppm)	R	electrical resistance (Ω)
V	volume of salt stream (mL)	A	cross-sectional area (m^2)
S	active area (cm^2)	L	height (m)
t	desalination time (s)	N	number of p-n couples in TEG
T_H	hot side temperature (K)	ΔT	temperature difference (K)
T_C	cold side temperature (K)	I	current (A)
$\overline{T}$	mean temperature (K)	U	voltage of desalination unit (V)
$z\overline{T}$	average ZT value	M_{NaCl}	molar mass of NaCl (58.44 g mol^{-1})
Q_H	input heat to hot side (W)		
Q_C	removal heat from cold side (W)	Subscript	
P_{out}	output electrical power (W)	p	p-type
α	seebeck coefficient (V K^{-1})	n	n-type
ρ	electrical resistivity (Ω m)	pn	p-n couple
λ	thermal conductivity (W m^{-1} K^{-1})	g	thermoelectric generator

The salt removal rate ($\overline{\nu}$, μg cm^{-2} min^{-1}) describes the average amount of salt removal per unit time during the entire desalination process, which can be expressed by the

following equation:[31, 32]

$$\bar{v} = \frac{(c_0 - c_t) \times V}{S \times (t/60)} \quad (1)$$

Thermoelectric conversion efficiency (η_1, %) is defined as follows:[33, 34]

$$\eta_1 = \frac{T_H - T_C\sqrt{1+z\overline{T}} - 1}{T_H \quad \sqrt{1+z\overline{T}} + \frac{T_C}{T_H}} \quad (2)$$

$$z\overline{T} = \frac{\alpha_{pn}^2 \times \overline{T}}{\rho_{pn} \times \lambda_{pn}} \quad (3)$$

$$\alpha_{pn} = \alpha_P - \alpha_n \quad (4)$$

$$\rho_{pn} = \rho_P + \rho_n \quad (5)$$

$$\lambda_{pn} = \lambda_P + \lambda_n \quad (6)$$

$$\overline{T} = \frac{T_H + T_C}{2} \quad (7)$$

Since the temperature difference ranging from 20 K to 65 K is small, temperature dependence of α, ρ and λ are assumed to be linear for the tested temperature interval.[35] In this case, the values of these quantities are taken at mean temperature.

Electricity utilization efficiency (η_2, %) refers to the percentage of electrical energy from TEG used for desalination, which can be obtained by following formulas:[36]

$$Q_H = \alpha_g I T_H + \mathrm{K}_g(T_H - T_C) - \frac{1}{2}I^2 R_g \quad (8)$$

$$Q_C = \alpha_g I T_C + \mathrm{K}_g(T_H - T_C) + \frac{1}{2}I^2 R_g \quad (9)$$

$$\alpha_g = N\alpha_{pn} \quad (10)$$

$$\mathrm{K}_g = N\mathrm{K}_{pn} = N(\mathrm{K}_p + \mathrm{K}_n) = N\left(\frac{\lambda_p A_p}{L_p} + \frac{\lambda_n A_n}{L_n}\right) = \frac{N(\lambda_p + \lambda_n)A_{pn}}{L_{pn}} \quad (11)$$

$$R_g = NR_{pn} = N(R_p + R_n) = N\left(\frac{\rho_p L_p}{A_p} + \frac{\rho_n L_n}{A_n}\right) = \frac{N(\rho_p + \rho_n)L_{pn}}{A_{pn}} \quad (12)$$

$$P_{out} = Q_H - Q_C \quad (13)$$

$$\eta_2 = \frac{\int_0^t UIdt}{\int_0^t P_{out}dt} \times 100\% \quad (14)$$

The physical parameters α, ρ, λ of p-type and n-type element under various test temperatures are displayed in **Table S1** in the Supporting Information.[37]

Thermoelectric utilization efficiency (η, %) is the product of thermoelectric conversion efficiency and electricity utilization efficiency:

$$\eta = \eta_1 \times \eta_2 \quad (15)$$

Heat consumption (E_H, MJ mol^{-1}) is an essential performance indicator to calculate the thermal energy requirement for removing one mole of NaCl during the desalination test, which can be obtained by the following equation:

$$E_H = \frac{\int_0^t Q_H dt \times M_{NaCl}}{(c_0 - c_t) \times V} \quad (16)$$

3. RESULTS AND DISCUSSION

3.1 The continuous desalination performance

Figure 2a shows the mechanism of redox flow desalination battery based on the temperature difference as driving force, and the device photo and detailed components are displayed in **Figure S1** in the Supporting Information. The TEG consists of 7 pairs of series connected p-n thermocouple. When the heater and air-cooling are started, a temperature difference is formed between the hot and cold sides of TEG, generating an electromotive force to power the desalination unit. The $[Fe(CN)_6]^{4-}$ ions are oxidized at anode by releasing electrons according to the equation (17), meanwhile, the released electrons are captured by the $[Fe(CN)_6]^{3-}$ ions in the cathodic reservoir through the external circuit, resulting in the reduction of $[Fe(CN)_6]^{3-}$ ions following the equation (18). With the help of ion exchange membranes, sodium ions in stream 2 are captured

by cathodic reservoir through the CEM at cathode side, and transported to anodic reservoir due to the connection of cathodic and anodic reservoirs, then released into stream 1 through the CEM at anode side, in order to maintain the ionic neutrality in both salt streams and the electrolyte. Simultaneously, chloride ions in stream 2 will be transported to stream 1 via the middle AEM. As a result, the salt in stream 1 is concentrated while the concentration of stream 2 decreases, as observed in **Figure 2b** which illustrates the variation in voltage and concentration of salt streams during the desalination process when a temperature difference of 65 K between the hot and cold sides of TEG is applied. The concentration in stream 2 decreased from the initial 5000 ppm to the final 344.3 ppm (93.1 % salt removal efficiency), yielding an average salt removal rate of 8.8 $\mu g \cdot cm^{-2} \cdot min^{-1}$. Combining with the current change from the initial 1.30 mA to the final 0.06 mA as the black curve shown in **Figure 2c**, the thermoelectric utilization efficiency (η) can be calculated to be 3.0 % with a thermoelectric conversion efficiency (η_1) of 3.5 % and a electricity utilization efficiency (η_2) of 85.4 %. It can be observed from the slope of the concentration curves in **Figure 2b** and **Figure S2** that the instantaneous salt removal rate is decreasing with the progress of desalination, because the reduced salt concentration in the diluted chamber increases the resistance.[38-41] The red curve in **Figure 2c** demonstrates a rising instant heat consumption due to a decreasing instantaneous rate of salt removal. The average heat consumption of whole desalination process is 284.3 $MJ \cdot mol^{-1}$, which is equivalent to completely burning 13.5 kg of waste from forestry such as sawdust and leaves to remove 1 mole of NaCl in saline water, given that the calorific value of wood is about 21 $MJ \cdot kg^{-1}$.[42]

Anode: $[Fe(CN)_6]^{4-} \rightarrow [Fe(CN)_6]^{3-} + e^-$ (17)

Cathode: $[Fe(CN)_6]^{3-} + e^- \rightarrow [Fe(CN)_6]^{4-}$ (18)

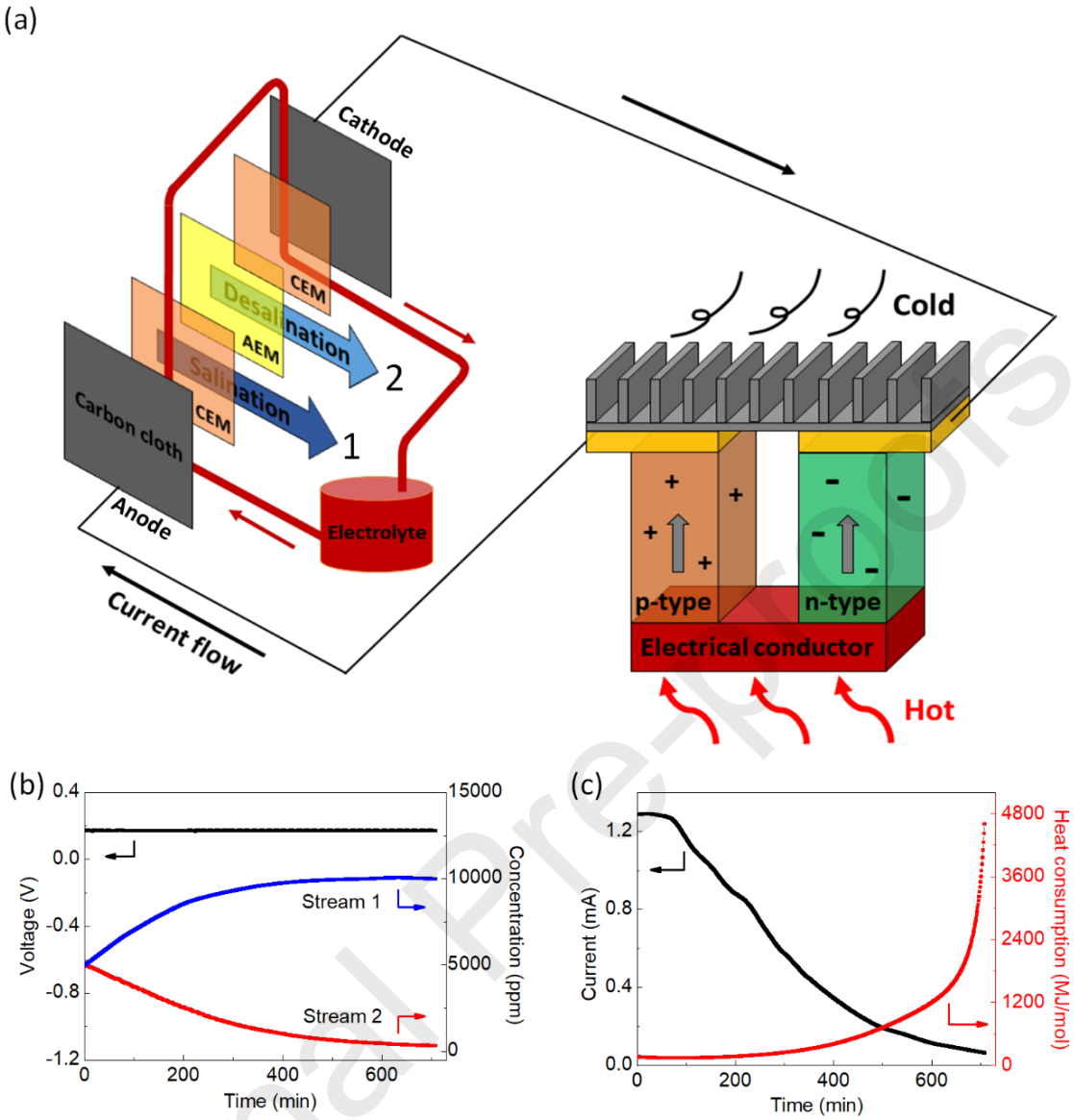

Figure 2. (a) The schematic diagram of the desalination system driven by temperature difference. (b) The variation in voltage and concentration of salt streams, (c) electrical current and instant heat consumption during the desalination process with the temperature difference of 65 K applied.

3.2 Impact of temperature difference on the desalination performance

The operation of desalination unit is driven by the temperature difference of thermoelectric unit. Thus, the temperature difference will have the great impact on the desalination performance. Herein, various temperature differences such as 20 K, 35 K,

50 K, and 65 K were tested. The changes of voltage and concentration of salt stream 2 are shown in **Figure 3a**. There is no obvious fluctuation in the voltage in each test, confirming that the system is very stable and durable at a constant temperature difference. But the voltage platform rises with the increase of temperature difference, which is consistent with the open-circuit voltage formula,[43] $V_{oc} = \alpha \times \Delta T$. The overall salt concentration of stream 2 keeps decreasing owing to the capture of both chloride ions and sodium ions by stream 1 reservoir and cathodic reservoir, respectively. During the identical period, the higher the temperature difference, the greater is the change in salt concentration, indicating a faster salt removal rate, as demonstrated in **Figure 3c**. The detailed comparison between concentration variation of two salt streams are displayed in **Figure S3a** and **Table S2** in the Supporting Information. The rate of salt concentration increase in stream 1 is experimentally close to the corresponding salt decline in stream 2.[44] It can be observed from **Figure 3b** that the original current of large temperature difference is higher on account of the higher voltage platform. Among the tested samples, the initial current is the maximum up to 1.3 mA with the temperature difference of 65 K while it is 0.64 mA at 20 K temperature difference. The total thermoelectric utilization efficiency (η) is obtained by multiplying the related efficiencies of thermoelectric conversion efficiency (η_1) and electricity utilization efficiency (η_2) in **Figure S3**, which reveals a growing trend in thermoelectric conversion efficiency[45] and electricity utilization efficiency. By reason of the high electromotive force at large temperature difference, **Figure 3d** exhibits a rising heat consumption as the temperature difference increases. The corresponding thermoelectric utilization efficiency is higher when consuming more heat under the condition of only changing the temperature difference.

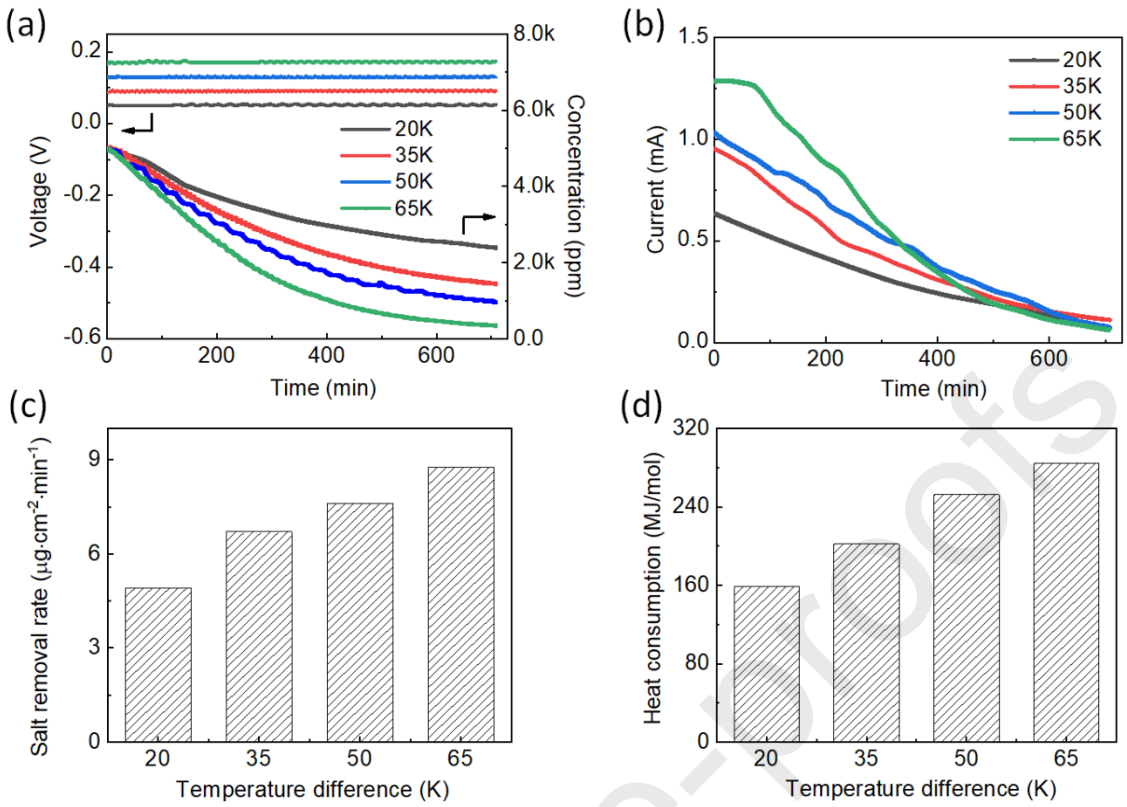

Figure 3. Changes of voltage and concentration in the diluted salt stream (a), and the corresponding current (b), the salt removal rate (c), and the heat consumption (d) under the various temperature differences.

3.3 The effect from the initial concentration of salt feeds

Since the concentration of salt feeds will affect the resistance and performance of the desalination device[46-50], it is necessary to investigate the influence from the initial concentration of salt feeds. For different initial concentration of salt feeds, the same concentration of NaCl is used as the conductive additive in electrolyte stream. **Figure 4a** depicts the changes of voltage and concentration of the diluted salt stream under the various initial salt feeds concentrations. During the tests, the temperature difference is equal to 65 K. As the initial concentration of salt feeds increases, the total resistance of the desalination device becomes smaller, while the electromotive force at the same temperature difference is maintained constant, thus the partial voltage inside the

desalination unit drops. It can also be seen from **Figure 4a** that the mean slope of the concentration curve in diluted stream rises with the increasing initial concentration of salt feeds, indicating a faster average salt removal rate as shown in **Figure 4c**. The data in **Table S3** and **Figure S4a** further proves that the salt growth rate in stream 1 roughly aligns with the salt removal rate in stream 2. Of the four tested samples, the initial current at a salt concentration of 7000 ppm is the largest in light of its lowest resistance, as observed in **Figure 4b**. The final current of all samples has dropped to approximate zero, and the eventual concentration of salt in stream 2 is around 340 ppm, which reaches the freshwater standard of 500 ppm. **Figure 4d** exhibits the variety in heat consumption per mole of salt removal in the initial salt feeds concentration range of the tested samples. As for the related efficiencies ($\eta, \eta_{1,}\eta_2$), it can be noticed from **Figure S4b-c** that the thermoelectric utilization efficiency tends to decline slightly with the increase of initial salt concentration because the low partial voltage on the device at high salt concentration makes the drop of electricity utilization efficiency while the thermoelectric conversion efficiency remains unchanged at the same temperature difference. In addition, the desalination test of high-concentration salt feed with 14000 ppm was carried out. The variation in voltage, concentration of diluted stream, and electrical current are demonstrated in **Figure S5**. It took 1935 minutes to reduce the salt feed concentration from 14000 ppm to 500 ppm, resulting in an average salt removal rate of 9.3 $\mu g \cdot cm^{-2} \cdot min^{-1}$. Based on the change curve of voltage and current, the thermoelectric utilization efficiency and average heat consumption can be obtained, which are 2.81 % and 268.0 $MJ \cdot mol^{-1}$ respectively. Hence, the redox flow desalination system based on the temperature difference is also suitable for the application in high salt feed concentration.

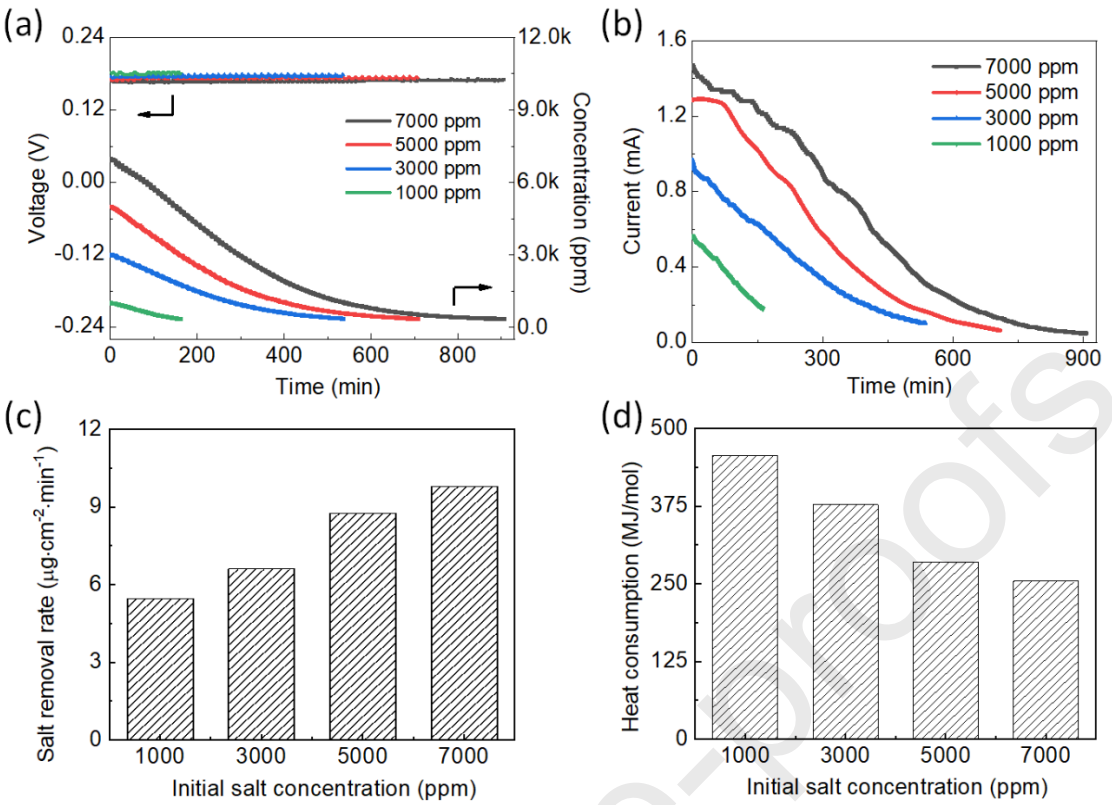

Figure 4. Changes of voltage and concentration of the diluted salt stream (a), and the corresponding current (b), the average salt removal rate (c), and the heat consumption (d) under different initial salt feeds concentrations.

3.4 The influence of electrolyte concentration

In order to study the influence of electrolyte concentration on the desalination behaviors, four sets of different electrolyte concentration tests were performed, i.e. 5 mM, 10 mM, 20 mM, and 40 mM, respectively, as demonstrated in **Figure 5**. The concentrated electrolyte can result in a slightly low voltage plateau and high initial current in desalination unit because of the low resistance[51, 52]. It can be seen in **Figure 5a** that the higher the electrolyte concentration is, the shorter the desalination time will be, thus causing a quicker average salt removal rate, which is consistent with the results in **Figure 5c**. In addition to the variety in the concentration of salt stream 2, the corresponding change of salt stream 1 is also shown in **Figure S6a**. Moreover, **Table**

S4 lists the average salt growth/removal rates in stream 1/2 at different electrolyte concentrations. In the tested samples, the least thermal energy is consumed when 40 mM/40 mM $[Fe(CN)_6]^{3-/4-}$ electrolyte applied, as demonstrated in **Figure 5d**, corresponding to the greatest removal rate. Furthermore, **Figure S6b-c** in the Supporting Information presents the related efficiencies (η, η_1, η_2). Except the same thermoelectric conversion efficiency, both electricity utilization efficiency and thermoelectric utilization efficiency get improved with the decrease of electrolyte concentration. Taking into account the desalination performances under different electrolyte concentrations, the $[Fe(CN)_6]^{3-/4-}$ solution of 20 mM/20 mM was selected as the redox electrolyte for the experiments in this work.

Therefore, under the condition of same temperature difference with different concentration of salt feeds or electrolyte, the current loaded into the desalination unit gets changed, causing a change in salt removal rate. As for the choice of redox couples, both metal salt electrolytes such as $Zn/ZnCl_2$ and non-metal organic electrolytes such as $TEMPO/TEMPO^+$ can be used in this thermo driving desalination system in principle, because they can all transfer electrons under the power drive. However, due to the excellent property of the rapid rate of electron transfer, ferri-/ferrocyanide redox couple can lead to a very low overpotential and require ultra-low energy consumption.[16] Hence, $[Fe(CN)_6]^{3-/4-}$ is selected as the redox mediator in our study.

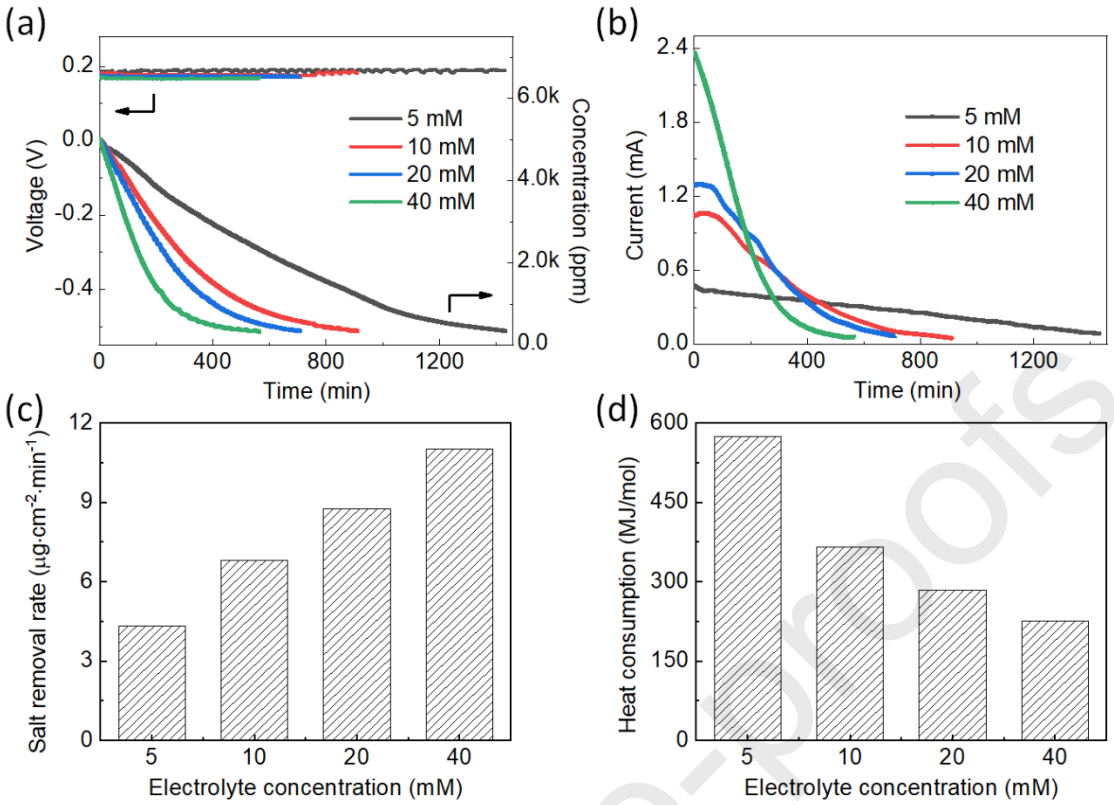

Figure 5. Changes of voltage and concentration of the diluted salt stream (a), and the corresponding current (b), average salt removal rate (c), and the heat consumption (d) under different electrolyte concentrations.

3.5 Cyclic desalination test

The cyclability is an important indicator to evaluate this system. To confirm the repeatability of the desalination process, four cyclic salt removal tests were conducted at the lab scale tests by replacing the salt feeds only and keeping the electrolyte unchanged. **Figure 6a-b** shows the change curves of voltage, salt streams concentration and electrical current during the four cycles, respectively. The salt concentration in diluted stream of each cycle is reduced from 5000 ppm to a freshwater baseline of 500 ppm. There are only negligible fluctuations in the corresponding curves during cycling, which proves the cyclability and stability of the system at the lab scale tests. Besides, the data of related desalination and thermoelectricity performance are summarized in

Figure S7. In order to further determine the compositional change of the electrolyte after cycling, the electrolytes before and after four cycles were detected by an ultraviolet-visible spectrophotometer and the absorption spectra are displayed in **Figure S8**. The position and intensity of the peak are basically remained, indicating no change in composition. Moreover, there are two limitations in the redox flow desalination on account of the use of redox electrolyte. One is the environmental contamination of some redox electrolytes[53]. The other is the limited lifetime of ion exchange membranes caused by the long-term contact with redox couples, resulting in a need to replace the membranes regularly[53]. These problems may be further improved by the development of membrane technology and the use of green electrolyte.

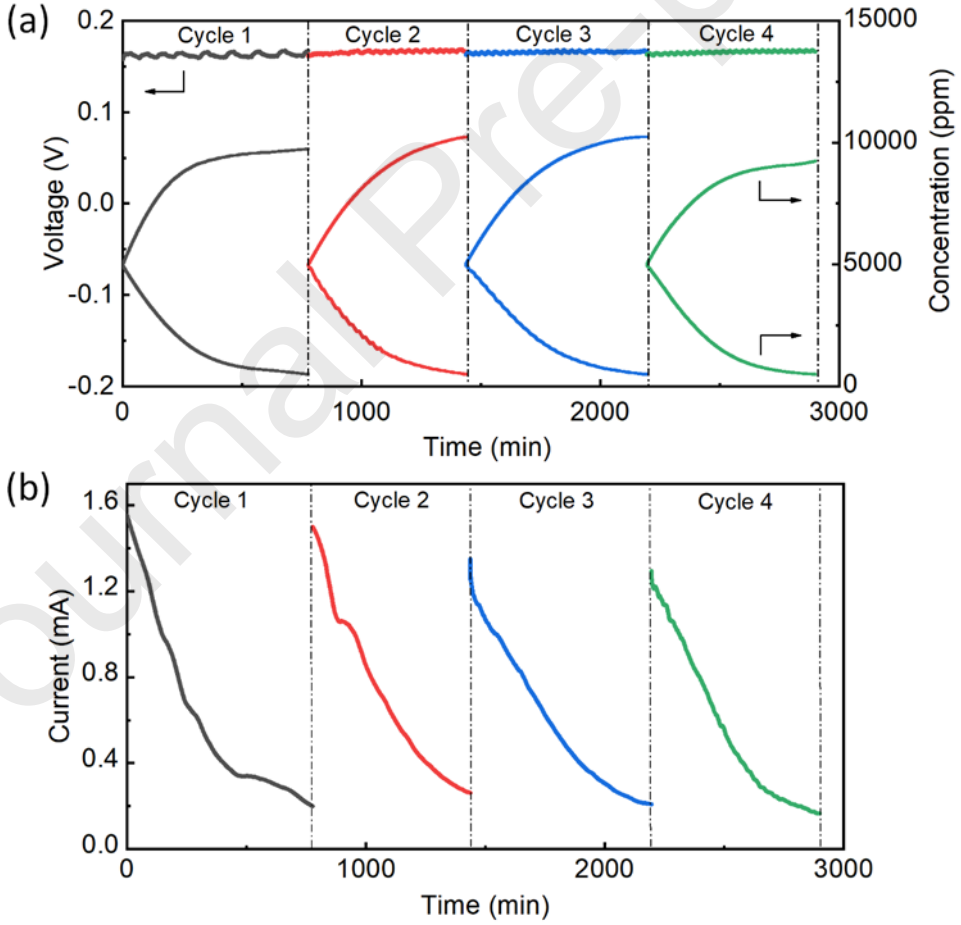

Figure 6. The variation of voltage, concentration of salt streams (a) during the four cycles, and the corresponding current change (b) under a temperature difference of 65

K.

4. CONCLUSIONS

In this work, a novel desalination system driven by temperature difference is put forward which uses the temperature difference to drive the redox flow desalination process. It is divided into two parts connected in series, one is a thermoelectric unit for power supply, and the other is a desalination unit for redox reactions. Under a certain temperature difference, the thermoelectric unit generates electromotive force and supplies it to the desalination unit of which the redox couples undergo the oxidation and reduction reactions with the movement of electrons, so that the ions in salt streams are transferred through the ion exchange membranes to achieve the coupling desalination. When a temperature difference of 65 K applied, the desalination system based on the temperature difference as the driving force can continuously process 5000 ppm salt stream to 344.3 ppm with a heat consumption of 284.3 MJ mol^{-1}, which reaches a salt removal efficiency of 93.1 % and an average salt removal rate of 8.8 μg cm^{-2} min^{-1}. Further, the efficiency performance related to this system has also been discussed in detail. Since the electrical driving force for desalination unit is generated by temperature difference, we consider to obtain various desalination performance by adjusting the temperature difference. In addition, the initial salt concentration and electrolyte concentration have a certain influence on the resistance of desalination unit and in turn affect the salt removal process. Therefore, the desired desalination effect can be achieved by changing the concentration of salt feeds and electrolyte.

This novel desalination system driven by temperature difference provides a new energy supply method for the electrochemical desalination with superior desalination performance. Owing to various sources of thermal energy, such as solar heat,

geothermal heat, waste heat, and combustion heat etc., the thermo driving desalination system can be practically used in many ways. For example, freshwater can be obtained to survive on natural scenes such as ships, islands, or ocean with temperature difference. The freshwater resources can also be produced in rural areas where electricity and water are lacking, and the waste heat from agriculture, forestry, or industry can be collected to provide a driving force for desalination process. It is believed that this method will be widely applied in the future desalination field with the development of efficient thermoelectric conversion materials.

ACKNOWLEDGMENTS:

This project was supported by National Key Research and Development Program of China (2019YFE0198000), Science and Technology Program of Guangzhou (2019050001), Scientific and Technological Plan of Guangdong Province (2018A050506078), the Department of Education of Guangdong Province (2019KZDXM014), Guangdong Provincial Natural Science Foundation (2016A030306033), National Natural Science Foundation of China (51978290), Project funded by Key-Area Research and Development Program of Guangdong Province (2019B110209002), the Outstanding Young Scholar Project (8S0256), the Science and Technology Development Fund, Macau SAR (File no. 0191/2017/A3, 0041/2019/A1, 0046/2019/AFJ, 0021/2019/AIR), University of Macau (File no.

MYRG2017-00216-FST and MYRG2018-00192-IAPME), and the UEA funding. F. Chen acknowledges the Pearl River Talent Program (2019QN01L951).

Supporting Information

The Supporting Information is available free of charge on the publication website.

REFERENCES

[1] B. Hu, Y. Zhang, Y. Li, Y. Teng, W. Yue, Can bioenergy carbon capture and storage aggravate global water crisis?, Science of The Total Environment 714 (2020) 136856.
[2] J.A. Añel, A.Y. Hoekstra, M.M. Mekonnen, A.K. Chapagain, R.E. Mathews, B.D. Richter, Global Monthly Water Scarcity: Blue Water Footprints versus Blue Water Availability, PLoS ONE 7 (2012) e32688.
[3] F. Yuan, Y.D. Wei, J. Gao, W. Chen, Water crisis, environmental regulations and location dynamics of pollution-intensive industries in China: A study of the Taihu Lake watershed, Journal of cleaner production 216 (2019) 311-322.
[4] Y. Chen, S. Wang, Z. Ren, J. Huang, X. Wang, S. Liu, H. Deng, W. Lin, Increased evapotranspiration from land cover changes intensified water crisis in an arid river basin in northwest China, Journal of Hydrology 574 (2019) 383-397.
[5] C. Craig, S. Feng, S. Gilbertz, Water crisis, drought, and climate change in the southeast United States, Land Use Policy 88 (2019) 104110.
[6] X. Zheng, D. Chen, Q. Wang, Z. Zhang, Seawater desalination in China: Retrospect and prospect, Chemical Engineering Journal 242 (2014) 404-413.
[7] H. Strathmann, Electrodialysis, a mature technology with a multitude of new applications, Desalination 264 (2010) 268-288.
[8] S. Al-Amshawee, M.Y.B.M. Yunus, A.A.M. Azoddein, D.G. Hassell, I.H. Dakhil, H.A. Hasan, Electrodialysis desalination for water and wastewater: A review, Chemical Engineering Journal 380 (2020) 122231.
[9] B. Wei, J. Feng, C. Chen, S. Zhong, S. Liao, Y. Yu, X. Li, Highly permselective tadpole-type ionic anion exchange membranes for electrodialysis desalination, Journal of Membrane Science 600 (2020) 117861.
[10] L. Bai, Y. Liu, A. Ding, N. Ren, G. Li, H. Liang, Fabrication and characterization of thin-film composite (TFC) nanofiltration membranes incorporated with cellulose

nanocrystals (CNCs) for enhanced desalination performance and dye removal, Chemical Engineering Journal 358 (2019) 1519-1528.
[11] D.-H. Nam, M.A. Lumley, K.-S. Choi, A Desalination Battery Combining Cu3[Fe(CN)6]2 as a Na-Storage Electrode and Bi as a Cl-Storage Electrode Enabling Membrane-Free Desalination, Chemistry of Materials 31 (2019) 1460-1468.
[12] D.-H. Nam, K.-S. Choi, Electrochemical desalination using Bi/BiOCl electrodialysis cells, ACS Sustainable Chemistry & Engineering 6 (2018) 15455-15462.
[13] J. Ma, Y. Cheng, L. Wang, X. Dai, F. Yu, Free-standing Ti3C2Tx MXene film as binder-free electrode in capacitive deionization with an ultrahigh desalination capacity, Chemical Engineering Journal 384 (2020) 123329.
[14] J. Ma, L. Wang, F. Yu, X. Dai, Mesoporous amorphous FePO4 nanosphere@Graphene as a faradic electrode in capacitive deionization for high-capacity and fast removal of NaCl from water, Chemical Engineering Journal 370 (2019) 938-943.
[15] Y. Park, D. Kang, K.S. Choi, Marked enhancement in electron-hole separation achieved in the low bias region using electrochemically prepared Mo-doped BiVO4 photoanodes, Physical chemistry chemical physics : PCCP 16 (2014) 1238-1246.
[16] F. Chen, J. Wang, C. Feng, J. Ma, T. David Waite, Low energy consumption and mechanism study of redox flow desalination, Chemical Engineering Journal 401 (2020) 126111.
[17] Q. Liang, F. Chen, S. Wang, Q. Ru, Q. He, X. Hou, C.-y. Su, Y. Shi, An organic flow desalination battery, Energy Storage Materials 20 (2019) 203-207.
[18] J. Wang, Q. Zhang, F. Chen, X. Hou, Z. Tang, Y. Shi, P. Liang, D.Y.W. Yu, Q. He, L.-J. Li, Continuous desalination with a metal-free redox-mediator, Journal of Materials Chemistry A 7 (2019) 13941-13947.
[19] Q. Zhang, S.H. Aung, T.Z. Oo, F. Chen, Continuous electrochemical deionization by utilizing the catalytic redox effect of environmentally friendly riboflavin-5'-phosphate sodium, Materials Today Communications 23 (2020) 100921.
[20] F. Chen, J. Wang, Q. Ru, S.H. Aung, T.Z. Oo, B. Chu, Continuous Electrochemical Desalination via a Viologen Redox Flow Reaction, Journal of The Electrochemical Society 167 (2020) 083503.
[21] D.H. Nam, K.S. Choi, Tandem Desalination/Salination Strategies Enabling the Use of Redox Couples for Efficient and Sustainable Electrochemical Desalination, ACS applied materials & interfaces 11 (2019) 38641-38647.
[22] F. Luo, Y. Wang, C. Jiang, B. Wu, H. Feng, T. Xu, A power free electrodialysis (PFED) for desalination, Desalination 404 (2017) 138-146.
[23] Q. Chen, Y.-Y. Liu, C. Xue, Y.-L. Yang, W.-M. Zhang, Energy self-sufficient desalination stack as a potential fresh water supply on small islands, Desalination 359

(2015) 52-58.
[24] M. Chen, Y. Mei, Y. Yu, R.J. Zeng, F. Zhang, S. Zhou, C.Y. Tang, An internal-integrated RED/ED system for energy-saving seawater desalination: A model study, Energy 170 (2019) 139-148.
[25] M. Haras, T. Skotnicki, Thermoelectricity for IoT – A review, Nano Energy 54 (2018) 461-476.
[26] V. Andrei, K. Bethke, K. Rademann, Thermoelectricity in the context of renewable energy sources: joining forces instead of competing, Energy & Environmental Science 9 (2016) 1528-1532.
[27] J.J. Black, T. Murphy, R. Atkin, A. Dolan, L. Aldous, The thermoelectrochemistry of lithium–glyme solvate ionic liquids: Towards waste heat harvesting, Physical Chemistry Chemical Physics 18 (2016) 20768-20777.
[28] D. Kraemer, K. McEnaney, M. Chiesa, G. Chen, Modeling and optimization of solar thermoelectric generators for terrestrial applications, Solar Energy 86 (2012) 1338-1350.
[29] Y. Zhang, S.K. Ravi, S.C. Tan, Food-derived carbonaceous materials for solar desalination and thermo-electric power generation, Nano Energy 65 (2019) 104006.
[30] Y. Zhang, T. Xiong, D.K. Nandakumar, S.C. Tan, Structure Architecting for Salt-Rejecting Solar Interfacial Desalination to Achieve High-Performance Evaporation With In Situ Energy Generation, 7 (2020) 1903478.
[31] J. Ma, C. He, D. He, C. Zhang, T.D. Waite, Analysis of capacitive and electrodialytic contributions to water desalination by flow-electrode CDI, Water research 144 (2018) 296-303.
[32] C. He, J. Ma, C. Zhang, J. Song, T.D. Waite, Short-circuited closed-cycle operation of flow-electrode CDI for brackish water softening, Environmental science & technology 52 (2018) 9350-9360.
[33] G.J. Snyder, E.S. Toberer, Complex thermoelectric materials, materials for sustainable energy: a collection of peer-reviewed research and review articles from Nature Publishing Group, World Scientific2011, pp. 101-110.
[34] G.J. Snyder, E.S. Toberer, Complex thermoelectric materials, Nature Materials 7 (2008) 105-114.
[35] S. Karabetoglu, A. Sisman, Z. Fatih Ozturk, T. Sahin, Characterization of a thermoelectric generator at low temperatures, Energy Conversion and Management 62 (2012) 47-50.
[36] M.C. Barma, M. Riaz, R. Saidur, B.D. Long, Estimation of thermoelectric power generation by recovering waste heat from Biomass fired thermal oil heater, Energy Conversion and Management 98 (2015) 303-313.
[37] R.L. Lidong Chen, Xun Shi, THERMOELECTRIC MATERIALS AND

DEVICES, 2018.
[38] G.M. Geise, A.J. Curtis, M.C. Hatzell, M.A. Hickner, B.E. Logan, Salt Concentration Differences Alter Membrane Resistance in Reverse Electrodialysis Stacks, Environmental Science & Technology Letters 1 (2013) 36-39.
[39] A. Galama, N. Hoog, D. Yntema, Method for determining ion exchange membrane resistance for electrodialysis systems, Desalination 380 (2016) 1-11.
[40] A.A. Moya, A Nernst-Planck analysis on the contributions of the ionic transport in permeable ion-exchange membranes to the open circuit voltage and the membrane resistance in reverse electrodialysis stacks, Electrochimica Acta 238 (2017) 134-141.
[41] A. Galama, D. Vermaas, J. Veerman, M. Saakes, H. Rijnaarts, J. Post, K. Nijmeijer, Membrane resistance: The effect of salinity gradients over a cation exchange membrane, Journal of membrane science 467 (2014) 279-291.
[42] E. Orémusová, L. Tereňová, R. Réh, Evaluation of the Gross and Net Calorific Value of the Selected Wood Species, Advanced Materials Research 1001 (2014) 292-299.
[43] L.C. Ding, A. Akbarzadeh, A. Date, Performance and reliability of commercially available thermoelectric cells for power generation, Applied Thermal Engineering 102 (2016) 548-556.
[44] J. Dai, J. Wang, X. Hou, Q. Ru, Q. He, P. Srimuk, V. Presser, F. Chen, Dual-Zinc Electrode Electrochemical Desalination, ChemSusChem 13 (2020) 2792-2798.
[45] K. Gaurav, S.K. Pandey, Efficiency calculation of a thermoelectric generator for investigating the applicability of various thermoelectric materials, Journal of Renewable and Sustainable Energy 9 (2017) 014701.
[46] P. Długołęcki, B. Anet, S.J. Metz, K. Nijmeijer, M. Wessling, Transport limitations in ion exchange membranes at low salt concentrations, Journal of Membrane Science 346 (2010) 163-171.
[47] S.M. Hosseini, S.S. Madaeni, A.R. Khodabakhshi, The Electrochemical Characterization of Ion Exchange Membranes in Different Electrolytic Environments: Investigation of Concentration and pH Effects, Separation Science and Technology 47 (2012) 455-462.
[48] D. Moreno, M.C. Hatzell, Influence of Feed-Electrode Concentration Differences in Flow-Electrode Systems for Capacitive Deionization, Industrial & Engineering Chemistry Research 57 (2018) 8802-8809.
[49] E. Yang, M.J. Choi, K.Y. Kim, K.J. Chae, I.S. Kim, Effect of initial salt concentrations on cell performance and distribution of internal resistance in microbial desalination cells, Environmental technology 36 (2015) 852-860.
[50] P. Długołęcki, P. Ogonowski, S.J. Metz, M. Saakes, K. Nijmeijer, M. Wessling, On the resistances of membrane, diffusion boundary layer and double layer in ion

exchange membrane transport, Journal of Membrane Science 349 (2010) 369-379.
[51] Y. Tian, J.-W. Yan, R. Xue, B.-L. Yi, Influence of electrolyte concentration and temperature on the capacitance of activated carbon, Acta Physico-Chimica Sinica 27 (2011) 479-485.
[52] Y. Zhao, M. Hao, Y. Wang, Y. Sha, L. Su, Effect of electrolyte concentration on the capacitive properties of NiO electrode for supercapacitors, Journal of Solid State Electrochemistry 20 (2015) 81-85.
[53] J.R. Varcoe, P. Atanassov, D.R. Dekel, A.M. Herring, M.A. Hickner, P.A. Kohl, A.R. Kucernak, W.E. Mustain, K. Nijmeijer, K. Scott, T. Xu, L. Zhuang, Anion-exchange membranes in electrochemical energy systems, Energy Environ. Sci. 7 (2014) 3135-3191.

Table of Content Graphic

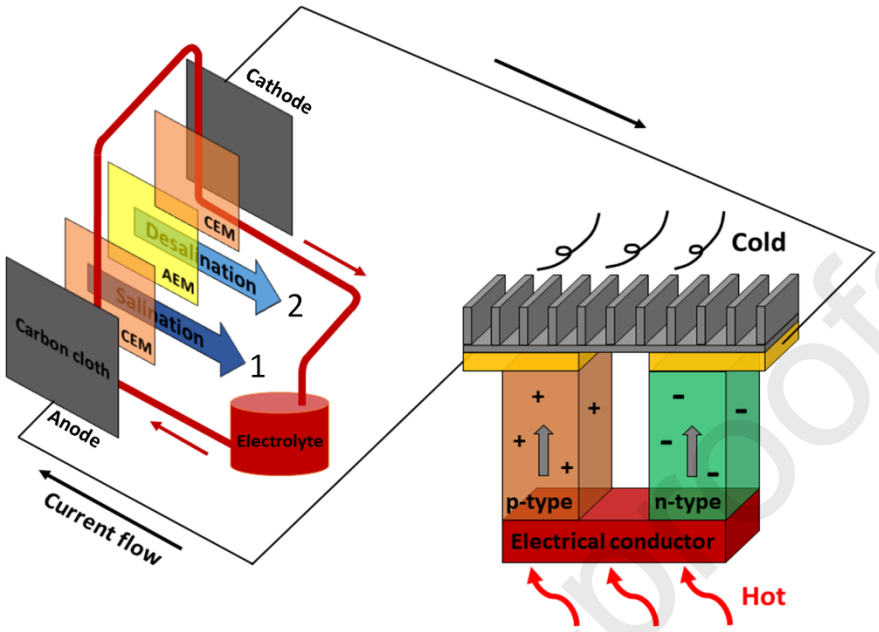

Highlights:

The redox flow desalination is driven by the thermoelectric power instead of off-the-shelf electricity.

The diluted water of 344.3 ppm can be obtained from initial 5000 ppm at 65 °C temperature difference.

The salt removal efficiency is up to 93.1 %.

The desalination performance can be controllable by adjusting the temperature differences.

Simple to assemble and operate the system outdoors.